FTIA publications
31/2021

Finnish Transport Infrastructure Agency

Research report on lidar detection performance of maritime navigation aids equipped with auxiliary reflectors

Tuomo Malkamäki, Afroza Khatun, Sanna Kaasalainen

Research report on lidar detection performance of maritime navigation aids equipped with auxiliary reflectors

FTIA publications 31/2021

Finnish Transport Infrastructure Agency
Helsinki 2021

Cover photo: FTIA photo archives

Verkkojulkaisu pdf (www.vayla.fi)
ISSN 2490-0745
ISBN 978-952-317-869-4

Finnish Transport Infrastructure Agency
P.O.Box 33
FI-00521 HELSINKI, Finland
tel. +358 (0)295 343 000

Preface

This research was prepared by Tuomo Malkamäki, Afroza Khatun and Sanna Kaasalainen at the Finnish Geospatial Research Institute FGI. The research was funded by the Finnish Transport Infrastructure Agency (FTIA). The contact person at the FTIA was Sami Lasma.

Helsinki May 2021

Finnish Transport Infrastructure Agency

Sisältö

1 Introduction

Lidar (light detection and ranging) technology has become increasingly prevalent in modern society. This technology has been adopted in various fields, such as ecological and geological surveying, robotics and industrial automation as well as autonomous vehicles. Recent decades have seen significant improvements in the performance, availability and cost of lidar equipment, driven largely by the need of various fields, like the autonomous vehicles. More recently, autonomous operation of maritime vessels has gained significant traction and hence, novel sensing methods to augment the traditional maritime radar has become of increasing importance. Lidar technology has been proposed as one of the leading solutions in improving, for example, situational awareness of maritime vessels and one of the key enablers of accurate maneuvering near harbors and other areas where traditional radars do not provide adequate accuracy [1]. Furthermore, lidars have already become common instrument in mapping maritime areas as well as for bathymetry in shallow waters.

Increasing use of the lidar in maritime applications raises a wide variety of research questions regarding performance and applicability to certain tasks. One such question is how well can lidars detect navigation aids used in maritime traffic, and whether there are steps that could be taken to improve this detection by better design of either the lidars or the navigation aids. In addition, lidar technology could be utilized, for example, in remotely surveying the condition of navigation aids.

This report summarizes research findings done on the detection of typical navigation aids used in national waters of Finland using lidar technology. The report includes results of lab measurements assessing optical properties of reflector materials used in navigation aids, as well as field tests of test targets measured with commercial lidars. In addition, the report examines related issues, like eye-safety and theoretical aspects in the detection of navigation aids.

2 Principles of lidar technology and limits of performance

Lidar technology utilizes light for measuring range between an instrument and a target. Majority of lidars utilize lasers as the light source due to the low dispersion and coherent nature of laser light. The range is typically detected by measuring the time it takes for a laser pulse to reach a target and reflect back to the lidar. Most commercial lidars use pulsed lasers, but lidars can also utilize continuous wave laser and measure the phase of the coherent echo reflected from the target. In addition to ranging, a scanning mechanism can be implemented, allowing the lidar device to construct two- or three-dimensional map of the surroundings, typically referred to as the point cloud. Furthermore, a lidar can measure the intensity of the light reflected back from the target in order to construct a more detailed point cloud which includes information on the reflectivity of the environment. In addition to the light source, lidars include receiver optics that focus the echo from the target onto a light sensor and signal processing circuitry that processes the digitized light signal. An example of a lidar, scanned target and the resulting three-dimensional point cloud with intensity information is depicted in figure 1.

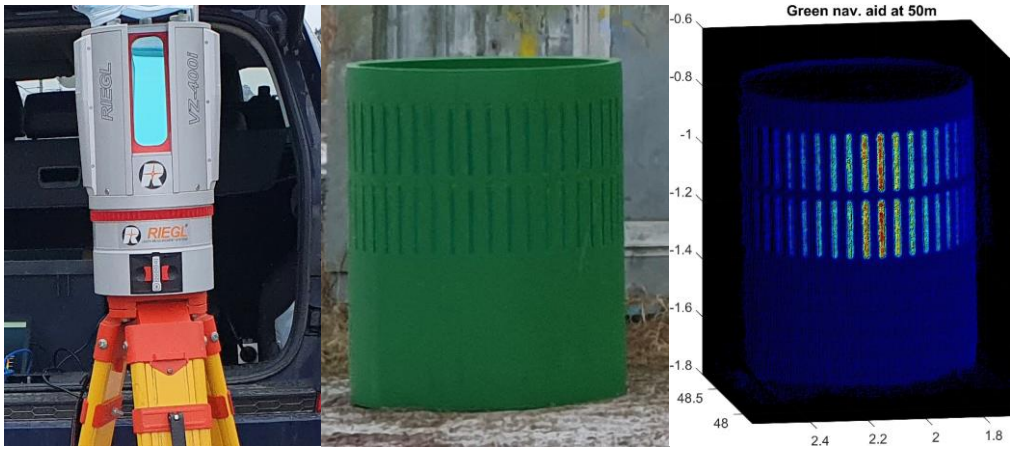

Figure 1: A state-of-the-art survey level lidar on a tripod is depicted on the left-hand side image. A target measured with the said lidar is shown in the middle. On the right-hand figure, the resulting point cloud is given, where the size of the target can be evaluated together with intensity of the reflections from the target. Each point in the point cloud represents a single laser pulse measurement.

Early implementations of 3D scanning lidars were based on some form of a gimbal that rotates the laser and optics. More modern implementations have used rotating mirrors with multiple laser transmitters to achieve somewhat limited resolution point clouds. Variations of these principles are in common use today. More novel technologies under active development today include flash lidars and optical beam steering where the scanning is implemented via electro-optical means. One scanning mechanism that has seen some commercial success recently is based on Risley prisms, where the independent rotation of two consecutive prisms allows scanning in a conical segment. Due to the needs of automotive industry, there is a significant push towards cost efficient and robust lidars and this is leading the field away from the traditional rotating optics. Number of applications, like geological

surveying will likely rely on traditional gimbal systems for the foreseeable future, largely due to high accuracy requirements.

The capability of a lidar to detect a target and measure the signal time-of-flight depends on the ability to measure the amount of light reflected from the target back to the lidar. Several factors impact this measurement:

- Laser output power and the divergence of the beam
- Attenuation of the laser beam and the echo in the medium (which typically is ambient air)
- Reflective characteristics of the target material
- Performance of the receiver optics
- Sensitivity of the optical sensor
- Signal processing methods
- Optical and electric noise

Laser output power is largely limited by the eye-safety requirements of commercially operated lasers and is typically on the order of milliwatts. The laser beam further experiences divergence and attenuation as it propagates in a medium. Beam divergence depends on the laser wavelength and characteristics of the focusing optics of the laser. Typical divergence values are around and below few milliradians. For example, a beam with a 3mm diameter at the laser output and a divergence of 0.35mrad, will experience an increase of 35mm in diameter for every 100m. As the beam diameter at a target (i.e. spot size) increases, significant portions of the light is typically lost due to irregularities or the shape of the target. For example, a target smaller than the spot size will only reflect a fraction of the pulse energy back towards the lidar, while bulk of the light flux continues to propagate forward and may eventually reflect from another target further away. Some of the modern lidars are capable of capturing several echo signals, given that the intensity of each echo is high enough for detection. Lidars equipped with simple signal processing will typically only report the highest intensity echo.

Attenuation of the signal in the atmosphere is impacted by molecular absorption and scattering as well as particle absorption and scattering. Molecular absorption is dominated by molecules in the air, such as carbon dioxide. This absorbance is highly wavelength dependent. Particle absorption and scattering occurs due to larger sized particles in the medium, e.g. various types of precipitation. Evidence seems to point that fog and similar weather phenomena are less wavelength dependant [2]. The optimal wavelength for lidar due to these various attenuation effects is heavily debated. Due to variation in e.g. the atmospheric conditions across the globe, there is not necessarily a single optimal solution. For most wavelengths, molecular absorption has relatively minor impact compared to adverse weather conditions like fog. Therefore, the wavelength selection of lidars should evaluate the importance of these adverse weather conditions, which significantly limit lidar measuring range. The wavelength selection is limited in practice by the available techniques for producing laser light. Typical wavelengths of commercial lidars operating in the infrared region are 840nm, 905nm, 1064nm and 1550nm. So called supercontinuum lasers produce ”white” light, which could be filtered for suitable wavelength, but this is not necessarily economically viable choice [3]. The laser wavelength also affect what types of surfaces can be detected as absorption and reflection of different materials depend on the wavelength. Water, for example, is highly absorbent at infrared wavelengths and water surface is, therefore, difficult to capture with lidars.

Reflections from targets depend heavily on the surface structure. Specular reflections occur at smooth, mirror type surfaces. Irregular surfaces produce diffuse reflections, scattering the light in a variety of directions. So called lambertian surfaces reflect incoming light evenly in all directions. The term reflectance is used to describe the ratio between incident and reflected light radiation and is often used to characterize material's optical behaviour. Since lidars can only measure the amount of light that is captured by the receiver optics, lidars can not measure true reflectance. As an example, a mirror surface can reflect most of the light, but direct it away from the lidar appearing as a very low reflectance target. Due to this, a term "backscattered reflectance" is often used with lidar measurements to emphasize the inherent shortcomings of the measuring technique [4].

Size and quality of the lidar receiver optics also play crucial role in the performance. A larger optical aperture enables to capture more of the reflected light flux and hence allow longer distance and the capability to detect targets with lower reflectance. Due to the beam divergence and typical reflection patterns, light flux received by a lidar is essentially inversely proportional to the square of the distance from a given target. Extending measuring range by increasing receiver optics size becomes impractical at some point as the increase required is exponential in nature. Emphasis is, therefore, typically put on the quality and precise alignment of the optics. High quality narrowband optical filters matched to the laser wavelength are commonly utilized to block radiation at all other wavelengths as the photosensors generally measure light intesity across a wide wavelength range and consequently, ambient light and other sources tend to interfere with lidar measurements. Photosensors are used in lidars to measure the light levels essentially by converting photons to electrons. Most commonly used sensor type is a so called avalanche photodiode, which can measure very minute light levels. Silicon photomultipliers are a novel sensor type which have seen significant improvements in recent years and are becoming attractive solution for lidars. Various sensor technologies utilize different semiconductor manufacturing processes and materials, which make them suitable for different wavelenths. Silicon based sensors operate generally in the visible to near infrared range of roughly 400-1000nm. InGaAs (Indium gallium arsenide) based sensors are used for infrared wavelengths. There are subtle differences in the noise levels of these different sensor types and moreover, in the efficiency and sensitivity to light. When discussing the wavelength selection of a lidar, photosensor sensitivy to a particular wavelength range is one of the major deciding factors. The two most common lidar infrared wavelengths, namely, 905nm and 1550nm, utilize different sensor materials and types and hence, any improvements to these sensor technologies could quickly make either wavelength superior choice for commercial lidars. Wavelength selection also dictates the amount of ambient light, which acts as a background noise when measured by the photodiode sensor. Amount of ambient light is higher at wavelengths which have less atmospheric attenuation and consequently, noise levels are higher at these wavelengths.

Light level measured by the photosensor is digitized and processed via electronics. In most simplistic form, echoes can be detected by evaluating when the light flux is above a certain predetermined threshold level. Significantly more complex and demanding approach is to record the light level output from the photosensor and identifying echo pulses from this signal. These so-called full waveform lidars allow significantly better performance at the expense of more complex electronics and processing. The accuracy at with which the time-of-flight, and hence, the distance to the target is defined, is highly dependent on the pulse processing method [3]. Also, state-of-the-art full waveform lidars can be used to detect material types based on the echo waveform.

In addition to the opto-electrical performance, the mechanical accuracy of the lidar is of significant importance. The accuracy with which the outgoing and echo pulse direction can be measured impacts directly the resulting point cloud accuracy. This accuracy becomes increasingly important as the measuring distance increases. For typical lidar operating ranges up to several hundred meters, existing solutions provide a decent accuracy. For kilometer range measurements, good accuracy in angular measurements is technically much more challenging to achieve. A 0.01° error in angular measurement result in roughly 17cm error at 1000m distance. Only a handful of commercial lidars provide millidegree level accuracy or better. Beam divergence exacerbates the point cloud deformation issues in combination with angular errors.

Another significant factor, especially in applications requiring fast point cloud acquisitions is the pulse rate of a lidar. Modern lasers are capable of producing millions of pulses per second. However, the pulse rate is limited by the time it takes for a single pulse to travel to the target and back. If a second pulse is sent before the echo of the previous pulse has returned, ambiguity is created as it is practically impossible to know (without making assumptions) which echo belongs to the first pulse. Pulse compression techniques utilized in radars to overcome ambiguity issues are yet not generally available for lidars. For a target at 1000m, the round-trip-time is roughly 6.6 microseconds, limiting pulse rate to 166kHz. This pulse rate limitation further impacts the density of pulses for a given scanning time and scanning space. If a sector of e.g. 45° x 45° is scanned in one second with a pulse rate of 1MHz, the angular resolution is 0.045°. At 100m, the distance between consecutive points would be roughly 8cm. For applications requiring long range and fast scanning of a given sector, gaps between consecutive points can become significant and smaller targets may be missed completely. For a given frame rate (i.e. frequency the scan of an area is repeated), the only practical solution is to utilize multiple lidars with smaller individual areas. Frame and pulse rate issues are important consideration for real-time applications, such as autonomous vessels.

Considering these various aspects, it is clear that high accuracy and long-range measurements are a challenging task for lidars, even with modern technology. This task can be alleviated by providing targets that are highly reflective and designed to maximize light reflected back at the lidar.

3 Evaluating navigation aid visibility for lidars

In order to evaluate suitability and performance of existing navigation aids and associated reflector materials for lidar detection, precise laboratory tests as well as field tests utilizing commercial lidars were carried out.

3.1 Laboratory tests

Laboratory tests were done in order to establish the reflector material characteristics. Specifically, the laboratory measurements were intended to assess the reflectance of the reflector materials over the wavelength range 800-1600nm encompassing the typical commercial lidar operating wavelengths. In addition, due to the retroreflective nature of the materials, the backscattered reflectance was measured across several different incidence angles with each angle scanned wavelenght wise over the 800-1600nm range. Furthermore, as the materials had a clear directional pattern, few different alignments of this pattern relative to the incoming light was studied across different incidence angles.

3.1.1 Materials

Evaluated materials were provided by two manufacturers, namely, 3M and Oralite. Four different visible color variants; red, green, blue and yellow were tested from each manufacturer and an additional silver colored version from Oralite. Detailed images of the measured reflector materials are depicted in Figures 2 and 3.

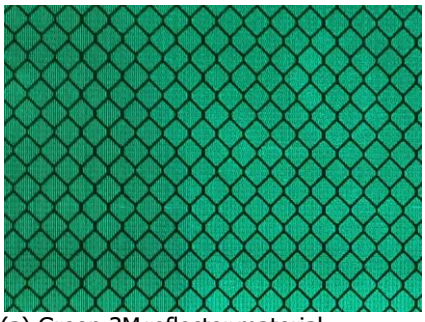

(a) Green 3M reflector material

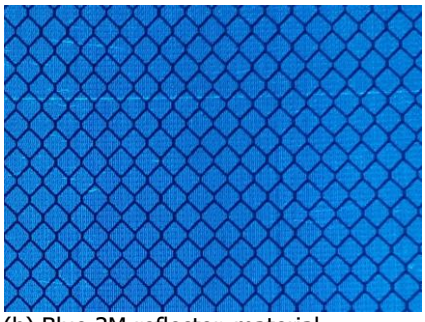

(b) Blue 3M reflector material

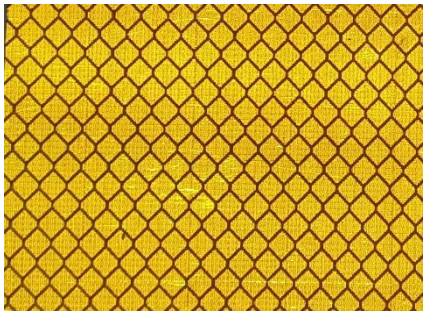

(c) Yellow 3M reflector material

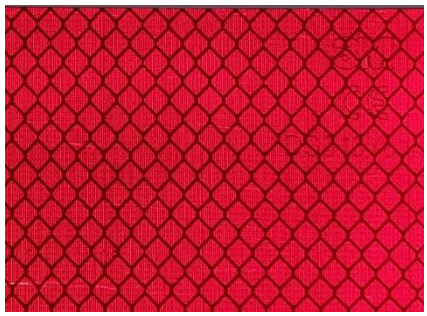

(d) Red 3M reflector material

Figure 2: Different color variants of the 3M reflector materials. There is a subtle difference in the reflector pattern between horizontal and vertical directions. Furthermore, there were subtle differences in the granularity of the pattern between different color variants.

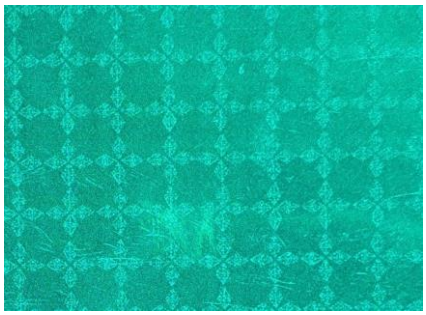

(a) Green Oralite reflector material

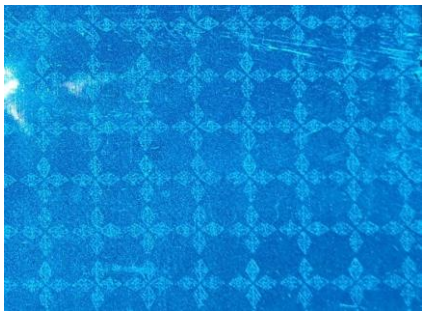

(b) Blue Oralite reflector material

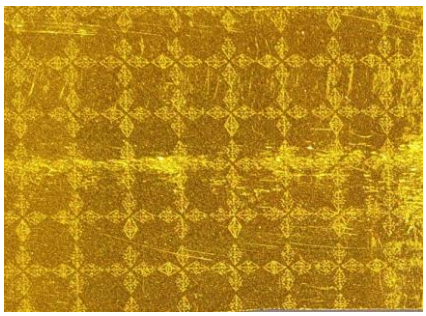

(c) Yellow Oralite reflector material

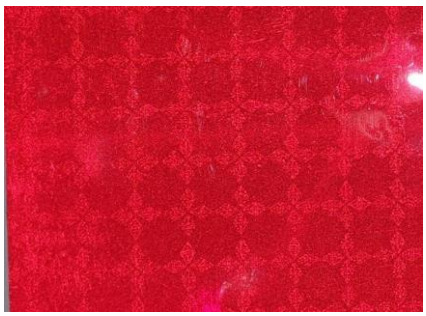

(d) Red Oralite reflector material

Figure 3: Different color variants of the Oralite reflector materials. Reflector patterns appear identical between horizontal and vertical directions.

All the materials had observable irregularities and some local scratching related to manufacturing tolerances and storing, transporting or handling of the material. Examining the materials revealed Oralite to have slight transparency passing small portion of light through the material, while 3M materials appeared totally opaque. For the measurements, the materials were cut to size by selecting high quality portions from the bulk material with as little irregularities and scratches as possible. Furthermore, handling the material was done in a way to avoid any contact with contaminating materials, including fingerprints.

3.1.2 Measurement setup

Reflectance measurements were carried out using the following equipment

- Newport broadband Quartz Tungsten Halogen (QTH) light source
- Oriel Cornerstone 260 extended range monochromator
- 4 inch Spectralon based integrating sphere
- Thorlabs PM400 power meter
- Thorlabs S122C photodiode

The monochromator is the central component in the setup and essentially functions as a narrow bandpass filter with a selectable center wavelength. By filtering a broadband light source, spectral range of the light output of the monochromator is within a narrow window centered around this selectable wavelenght. The width of this wavelength window (i.e. resolution) depends on the particular grating or prism type and the input and output slit widths used in the monochromator. Aiming the filtered light from the monochromator output to a target material and measuring the intensity of the light reflected off the target allows to establish the spectral reflectance of the material at that wavelength (within the finite wavelength resolution). Scanning over a wavelength range and

measuring light intensity at each wavelength allows then to establish spectral response of a material across a wide wavelength range.

In practice, light from the QTH source was passed through either a 650nm or a 950nm longpass optical filter element to the monochromator input port. Filtering of the light source was done in order to block higher order (i.e. shorter) wavelengths from passing through the grating based monochromator. Filtering is common in gratings based monochromators, in which the output contain second and third order harmonics (i.e. half and one third) of the intended output wavelength, due to the nature of gratings. The 650nm longpass filter was used when operating the monochromator below 1050nm and the 950nm filter was used above 1050nm. The monochromator was equipped with input and output slit widths that provide 4.9nm wavelength window at the output of the monochromator. The monochromator was used by sliding this 4.9nm wide wavelength window in 1nm steps from 700 to 1800nm. Output from the monochromator was collimated by an off-axis parabolic mirror in an integrating sphere system which aimed the light at the reflector material under test placed at the sample port of the integrating sphere. Use of integrating sphere is standard practice in reflectance measurements. It allows to collect majority of the light reflected from the target and focus it on a measuring device. This is accomplished via highly reflective material, typically Spectralon, with which the internal cavity of the integrating sphere is coated. Spectralon provides around 99% reflectivity across large range of wavelengths with negligible spectral impact. A high precision photodiode power sensor was used at the integrating sphere output port to capture the light intensity level which was then digitized via the power meter. The measurements were automated by running a customized software controlling the monochromator wavelength and logging the power meter readings. 100 intensity samples were collected at each wavelength step and later averaged in the analysis stage for each material. To remove the spectral characteristics and response of the monochromator, light source and photodiode, a reference measurement was made using Spectralon sample. This reference measurement was then used at the analysis stage to normalize target material measurements. The integrating sphere together with material and photodiode placement is depicted in figure 4.

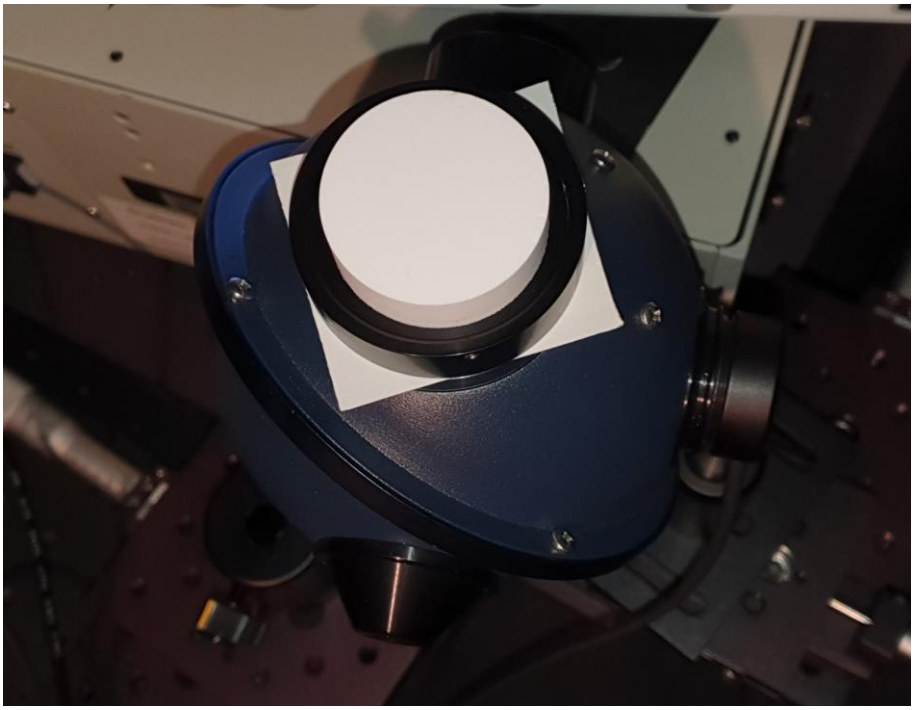

Figure 4: Integrating sphere used in the reflectance measurements. Photodiode sensor is placed at the output port on the right side of the sphere. Small square of the sample material is placed at the output port of the sphere, here seen at the top. A weight with a flat surface was placed on top of the sample to provide tight seal around the sample and to even out any curvature in the material. The weight seen here is a special end cap with a white Spectralon surface, which was used in place of the sample for the reference calibration. Light from the monochromator, which can be seen in the background, enters the sphere from the bottom, via the parabolic collimating mirror.

Measurements evaluating the impact of incidence angle were carried out using the same light source, monochromator and power meter as in the reflectance measurements. However, the integrating sphere was replaced by a 3 inch 90° off-axis parabolic mirror in order to mimic the typical lidar collection optics. Light output from the monochromator was passed through a hole in the parabolic mirror (the hole being coaxial to the collimating axis of the mirror) to the target material. The target material was placed on a precision rotation stage, which allowed accurate incidence angle control. Backscattered light from the target was collected via the parabolic mirror and focused on to an optical fiber propagating the light to a photo-diode.

For reference, the components used in incidence angle measurements are listed below.

- Newport broadband Quartz Tungsten Halogen (QTH) light source
- Oriel Cornerstone 260 extended range monochromator
- Thorlabs PM400 power meter
- Thorlabs S145C photodiode
- Thorlabs 3 inch aluminium parabolic 90° off-axis mirror
- Newport URS75BCC precision rotation stage and SMC100CC controller

The parabolic mirror setup and the rotation stage with a target material attached are depicted in figure 5.

In addition to the rotation stage controlling the incidence angle formed by the incoming light beam path and the surface normal of the target material plate, an additional rotation of the target material around the surface normal was accomplished by hand. A right-angle ruler was used to align this target material rotation angle within few degrees of accuracy.

The setup was automated to scan the wavelength range from 700 to 1800nm with 2nm steps. Incidence angle was automatically incremented with 5° steps from 0° to 65° after each wavelength scan. 30 intensity readings were recorded at each wavelength step and averaged in the post-processing of the data. This measurement was repeated for the few different rotational alignments of the target materials. Namely, 3M material were measured with 0°, 45° and 90° alignments. Oralite material was measured with 0° and 45° alignments. The distance from the parabolic mirror focusing axis to the target material plane was set to 3m with a measuring tape. The shape of the light beam projected on the target plane at 0° incidence angle was roughly 2cm wide and 6cm high. The size was a compromise between reasonably small beam divergence, adequate target illumination size and light intensity levels across the measurement parameters. In essence, this spot size and shape allowed the light flux projected at the target to remain constant throughout the varying incidence angles and captured more than one spatial cycle of the repeating reflector patterns, while minimizing the spread of the light beam. The incidence angle measurements were carried out in darkened conditions with additional light blocking surfaces over the measuring setup in order to avoid any stray light interfering with the measurements.

Figure 5: Essential optical components and setup for the incidence angle measurements. Blue target sample is placed on the precision rotation stage seen at the top of the picture. Rotation stage allows incidence angle variation (i.e. rotation around vertical axis) relative to the incoming light beam. The light beam from the monochromator passes through a hole in the parabolic mirror seen at lower right hand side of the picture. Light reflected from the target is then focused by the mirror on to a optical fiber attached to a positioner seen at the lower left. This fiber propagates the light to a photodiode for measurement.

3.1.3 Results

Reflectance measurements implemented using the integrating sphere exhibited relatively constant spectral response for all the materials across the measurement range from 700-1800nm. The sensitivity of the photodiode used in the measurement decreases towards the edges of the nominal measurement range of 700-1800nm. Consequently, measurements between 700-800nm were relatively noisy and were removed from the analysis. The measured reflectances of the materials are depicted in Figures 6 and 7, respectively, for 3M and Oralite.

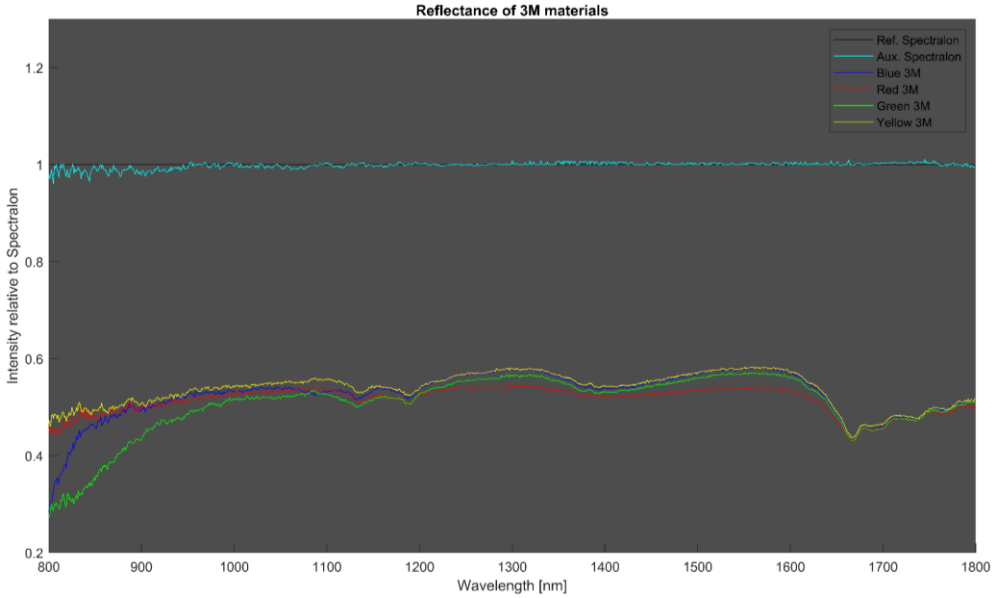

Figure 6: Reflectance of the 3M materials. Each value is normalized against Spectralon reference (black line with a constant intensity of 1). Auxiliary Spectralon measurement (cyan) was done in order to evaluate repeatability and error values at different wavelengths. The sensitivity of the photodiode used in the measurements decreases towards both ends of the wavelength range and hence, measuring noise is pronounced near the edges.

The resulting reflectance graphs show slight variation between the different color variants within each manufacturer. Differences in the 3M color variants are more pronounced, compared to Oralite, for which all the color variants exhibit almost identical reflectance.

Differences between materials from different manufacturers are more profound with 3M materials exhibiting slightly higher reflectance between 900-1600nm. Above roughly 1650nm, Oralite appears to have slightly higher reflectance. However, notable observation from the results is that materials from both manufacturers have significantly lower reflectance compared to the Spectralon reference. Namely, both materials exhibit roughly half the reflectance of Spectralon. Considering that the target materials are designed to be reflective, this may seem somewhat unexpected. One significant reason for the lower reflectance is likely attributable to the retroreflective nature of the target materials. Due to this, a portion of the light reflected by the target is likely directed back to the monochromator and hence, not measured by the photodiode. Consequently, the results need to be evaluated against the incidence angle measurements.

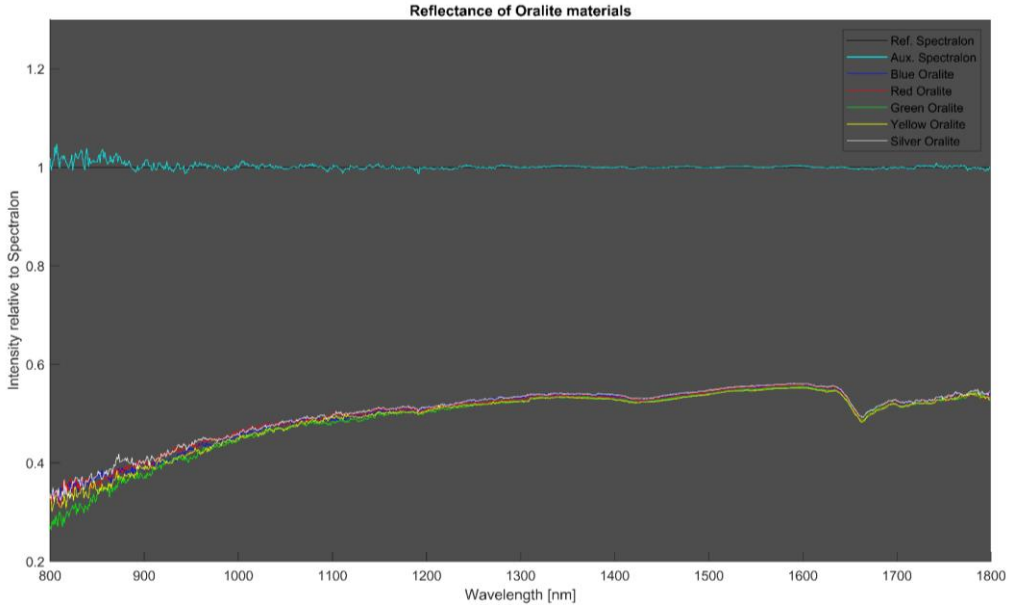

Figure 7: Reflectance of the Oralite materials. Each value is normalized against Spectralon reference (black line with a constant intensity of 1). Auxiliary Spectralon measurement (cyan) was done in order to evaluate repeatability and error values at different wavelengths. The spectral response of the photodiode used in the measurement decreases towards both ends of the measurement range and hence, noise is increased at the edges.

Results from the incidence angle measurements are summarized in figures 8 and 9. These figures express intensity of backscattered reflectance at various incidence angles normalized with intensity of the particular sample at 0° angle. These values are average over the 800-1600nm range. More thorough results showing intensities as a function of wavelength, and for various incidence angles are depicted in appendices A.1 for 3M and A.2 for Oralite.

Observing figure 8, we can notice that for 3M materials, there are subtle but observable differences between different pattern alignments. With 0° rotation angle, the intensity drops more rapidly, compared to the other alignments. This indicates that 3M materials disperse or scatter light in spatially non- homogeneous way. Hence, the retroreflective performance varies depending on the spatial direction relative to the reflector pattern. This directional behaviour can also be observed from the figures in appendix A.1. Based on these figures it can be concluded that 3M materials tend to exhibit exponential decay with 0° alignment, whereas the decay is much more linear with 90° alignment. 3M materials aligned with 45° show mixed results. Yellow 3M material appears to have less predictable behavior as the backscattered reflectance is relatively high for incidence angles around 10-30° and furthermore, has higher variation across the wavelength range.

Oralite materials, on the other hand, perform much more uniformly and appear to have relatively linear decay in backscattered reflectance intensity as the incidence angle increases. This indicates better retroreflective performance at higher incidence angles, compared to 3M materials. However, as these values are normalized against each material's 0° values, these values can not be used for absolute reflectance comparison between manufacturers. For this purpose, Oralite materials were normalized with 3M blue target material with 0° alignment. These results are depicted in appendix A.3. In absolute terms, 3M exhibits higher

reflective performance, as the absolute intensity values of Oralite are observably lower between 900-1600nm wavelengths for 0° incidence angle.

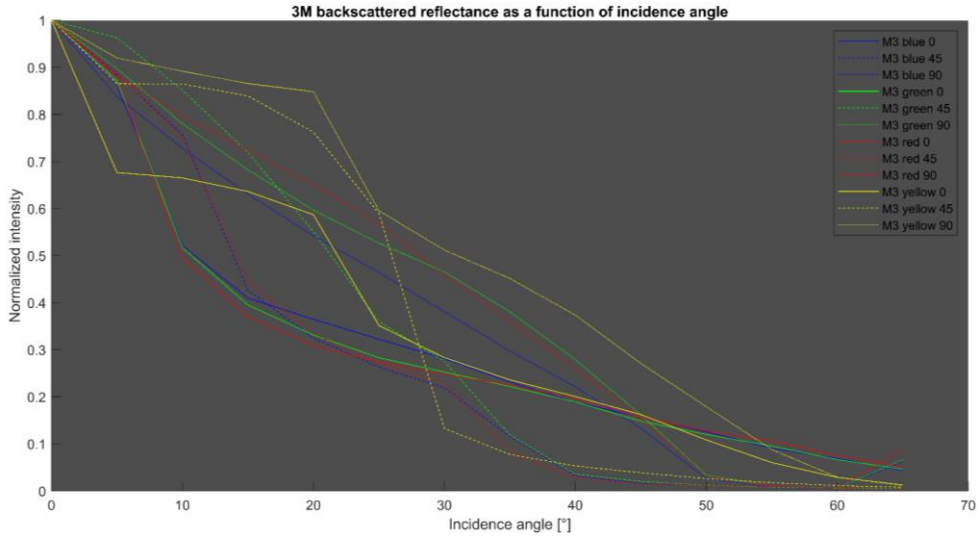

Figure 8: Backscattered reflectance from the 3M materials with varying incidence angles and for three different rotational alignments of the materials (0°, 45° and 90°). For blue, green and red t 0° rotation, backscattered reflectance decreases rapidly as incidence angle increases, indicating relatively high retroreflective characteristics. Decrease in reflectance is approximately exponential. However, yellow 3M material exhibits above expected reflectance between 10-20° incidence angles. For 45° and 90° alignments, backscattered reflectance drops less rapidly and there are more observable differences between materials.

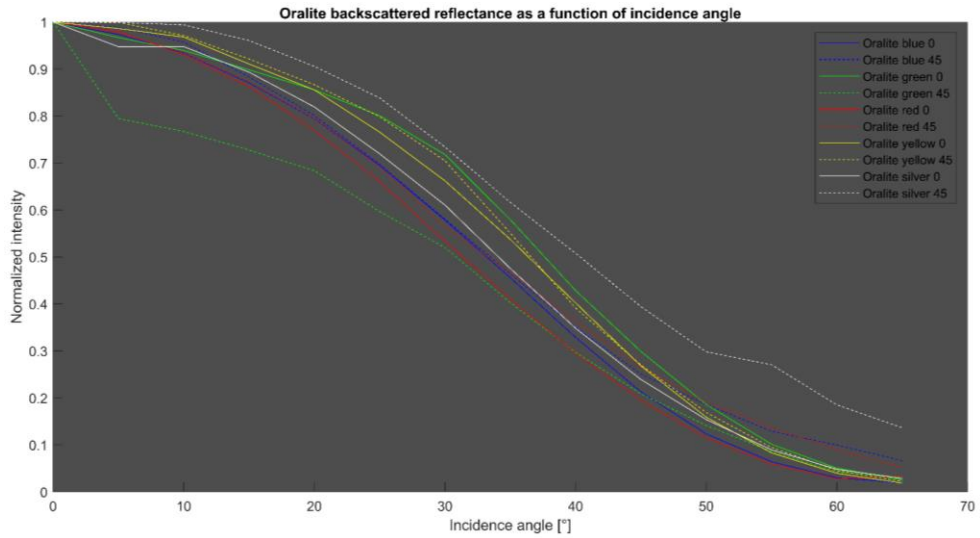

Figure 9: Backscattered reflectance from the Oralite materials with varying incidence angles and for two different rotational alignments of the materials (0° and 45°). For all color variants, the reflectance decreases less rapidly compared to 3M. It should be noted that these values are normalized to the 0° incidence angle of each variant and do not present absolute intensity values.

3.2 Field tests

Field tests utilizing commercial lidars were implemented in order to assess how actual navigation aids with embedded reflector material are seen by lidar scans. From early field and laboratory evaluations of the targets and reflector materials, it became evident that the targets will be visible well beyond the range of most commercial lidars operating typically below 300m. For this reason, the study focused specifically on evaluating longer range detection, beyond 300m. Capability to detect maritime targets beyond short range is of great practical importance due to e.g. maneuverability of larger vessels.

3.2.1 Targets

Five different navigation aid test targets were provided for evaluation. These were segments from real navigation aids currently utilized across Finnish national waters. These varied in diameter, between 16cm up to 80cm, and also in the visible color of plastic base material. Each target had CNC-milled grooves, in which narrow strips of 3M reflector material presented in previous chapter was embedded. Due to practical reasons, e.g. transportability, the targets were cut down segments, rather than full size navigation aids. The five different navigation aids are depicted in figure 10. These will be referred to by the reflector color. Specifically, the black navigation aid with blue reflectors will be called ”blue navigation aid”

Based on preliminary tests, both in the lab and in the field, the plastic base material of the targets had dispersive characteristics similar to Lambertian surfaces. Hence, the plastic materials would be much less visible to lidars, compared to the reflector materials.

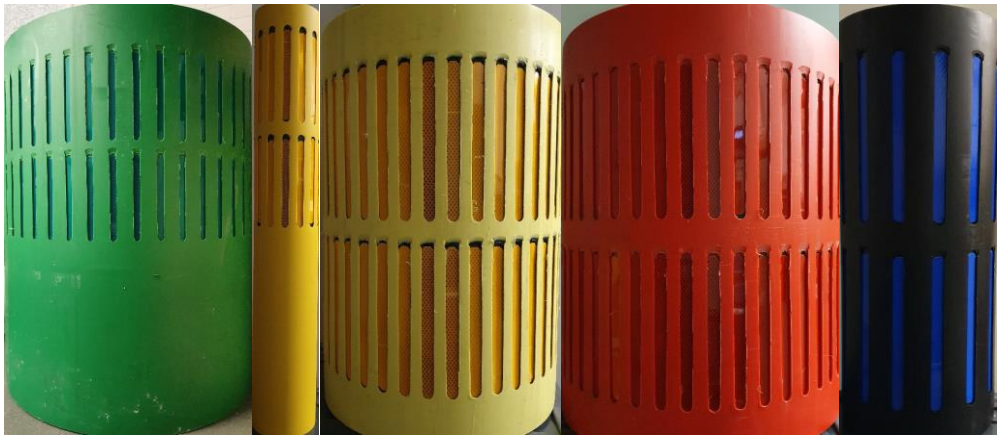

Figure 10: Navigation aid sections used in the field measurements:
(a) Green, 80cm diameter navigation aid
(b) Narrower, 16cm diameter yellow navigation aid
(c) Wider, 40cm diameter yellow navigation aid
(d) Red, 50cm diameter navigation aid
(e) Black, 22cm diameter navigation aid with blue reflectors

3.2.2 Measurement setup

The five navigation aid targets were placed on the ground spatially separating them by several meters. Figure 11 depicts the placement of the targets. In addition to the navigation aid targets, several reference targets were placed in the vicinity of the targets. These references include a 4-shade Spectralon plate and matte aluminium plate. Behind the targets were a large metallic structure which provided further reference.

Figure 11: Placement of the navigational aids and references used in the field tests. 4-shade Spectralon plate is placed on the upper left side of the wall of background structure. Brushed aluminium plate was placed in front of the targets and is seen in the right of the center, in the bottom of the picture.

Selection of lidars capable of operating beyond the 300m range is severely limited. A summary of a selection of commercial lidars with typical characteristics can be found in [1]. After careful evaluation, two long range lidars were selected for the field measurements, namely, Riegl VZ-400i and Livox Tele-15. They were selected in order to cover the two most commonly used wavelengths (905nm and 1550nm), two different scanning mechanics and opposite ends of the cost and quality range. Top of the class Riegl VZ-400i is a survey level lidar capable of very accurate measurements up to and beyond 800m range. VZ-400i is designed for precision scanning in mostly stationary setups. It performs full waveform analysis and has advanced features for survey type of tasks with emphasis on usability and efficient post-processing of large point cloud datasets. Livox Tele-15 is a long range, highly cost-efficient device aimed mostly at OEM-, automotive and robotics markets with range up to 500m. This range is extendable to 1000m with custom firmware which was not available at the time of the field tests. Tele-15 utilizes Risley prism type of scanning mechanics and is geared towards real-time applications with very minimal usability functionality ”out-of-the-box”. Basic specifications for the two lidars used are collected in table 1.

In both lidars, the pulse rate is largely limited by the measuring distance. Riegl can increase the pulse rate at the expense of decrease in measuring distance.

Table 1. Specifications of the two lidars used in the field measurements.

	Riegl VZ-400i	**Livox Tele-15**
Scanning area (FOV)	100° x 360°	14.5° x 16.2°
Laser wavelength	1550nm	905nm
Laser safety	Class 1	Class 1
Range precision	<5mm @ 100m	<2cm @ <220m, 80% reflectivity <4cm @ <120m, 10% reflectivity
Pulse rate	up to 1.2MHz 100kHz @ 800m range	240kHz
Beam divergence	0.02° (0.35mrad)	0.02° x 0.12° (0.35 x 2.1mrad)
Angular resolution	<0.0007°	<0.03°
Range	800m @ 90% reflectivity 400m @ 20% reflectivity	500m @ 50% reflectivity 320m @ 10% reflectivity

For Livox, also the beam divergence likely limits meaningful measurements much beyond the 500m range. Given the beam divergence of 0.35mrad, each additional 100m in distance increases the beam diameter by 35mm. Hence, for Riegl with a beam diameter output of 3mm, the spot size diameter is 38mm at 100m, 73mm at 200m and 266mm at 750m distance. For the Livox with ellipsoidal beam, the hori- zontal beam width follows Riegl, while the vertical size increases from 213mm at 100m to 1053mm at 500m.

Measuring of the targets was accomplished by starting from 50m distance and moving the lidars farther from the targets in 50m steps. Distance between each measuring location was ensured using measuring tape. Measurements with Livox was stopped at 500m and Riegl at 750m. Angular scanning precision of the Riegl lidar was increased as the distance to the targets grew, in order to keep the point density roughly equal at different distances. With livox, the resolution is constant and hence could not be changed. Furthermore, due to the conical scanning pattern of the Risley prism system, the point cloud density is higher in the center of the Livox scanning cone. Consequently, the livox was carefully aimed at middlemost navigation aid at each distance step. The two lidars during the measurements are depicted in figure 12, mounted on tripods.

Figure 12: The two lidars used in the field tests mounted on tripods. Livox lidar is placed on the left side, while Riegl is placed on the right.

3.2.3 Results

Point cloud data collected during the field measurements was post-processed and analyzed. The overall target area, as well as each individual target was cropped from the full point clouds at each distance. Detailed images of these point clouds can be found in appendix B.1 for Riegl and appendix B.2 for Livox.

From the processed point clouds, 20 highest intensity points were selected and averaged to get average peak amplitude for each target. This average amplitude is depicted in figure 13 as a function of distance for each target and the aluminium reference plate. The amplitude follows the typical exponential decay. The navigation aid targets exhibit significantly higher echo amplitude compared to the aluminium reference. The navigation aids show almost identical curves. However, we can observe that blue, green and short yellow targets show slightly lower echo amplitude for all distances, compared to almost identical amplitudes shown by red and the longer yellow targets. Difference in the amplitude may be partly explained by plastic base and reflector materials of the navigation aids. However, more likely explanation for this difference is the density and specifically the incidence angles of the embedded reflectors. Considering the figure 10, we can observe that in green and blue navigation aid, the density of the reflectors is lower. This essentially makes it less probable to have a reflector close to 0° incidence angle relative to the beam. While the reflector density in the long yellow aid is similar to the short yellow and red aids, the angle between adjacent reflectors is higher due to the narrow diameter of the aid. Hence, the short yellow and red navigation aids have higher probability of having reflectors with low incidence angles, when moving the lidar relative to these targets.

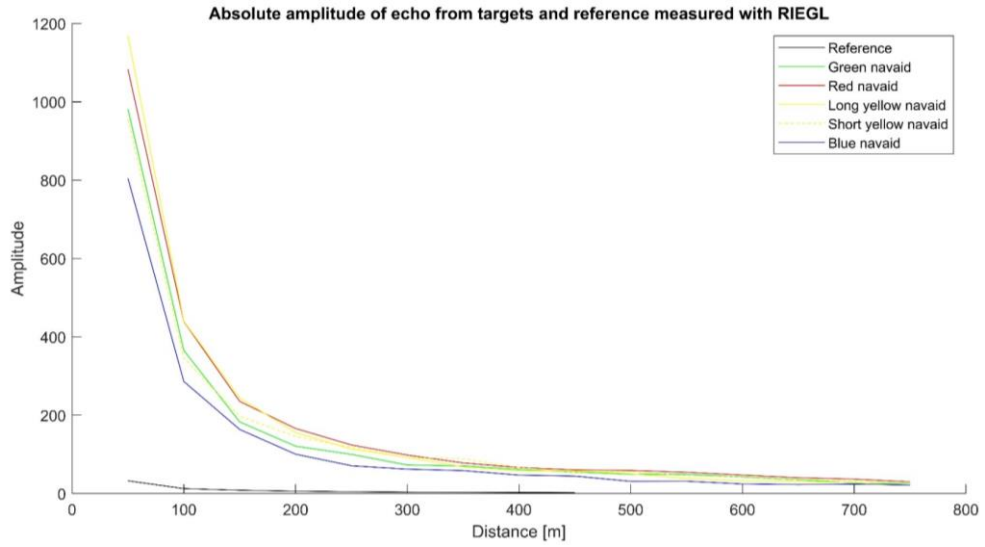

Figure 13: Riegl records both the absolute amplitude of the echo, as well as distance corrected reflectance. Absolute amplitudes from the targets and reference shown here as a function of distance follow the typical exponential decay. Non-negligible differences between the targets can be observed, as echoes from blue appear to be attenuated the most. Green and short yellow are also observably below the amplitudes of both, long yellow and red target, the two of which are seemingly almost identical.

Riegl records absolute amplitude of the echo pulse and calculates distance calibrated reflectance based on the amplitude and pulse shape. Description of the relationship between amplitude and distance calibrated reflectance of the Riegl can be found in [5]. Reflectance values produced by the Riegl are depicted in figure 14. Observations similar to the amplitude can be made from the reflectance figures, as the blue and green navigation aids show significantly lower reflectance. Fluctuation in the reflectance values may be partly explained by difference in the density of the reflectors and the consequent alignment of the reflector surface normals to the incident beam. The impact of the Riegl internal calibration algorithm is unknown at this stage.

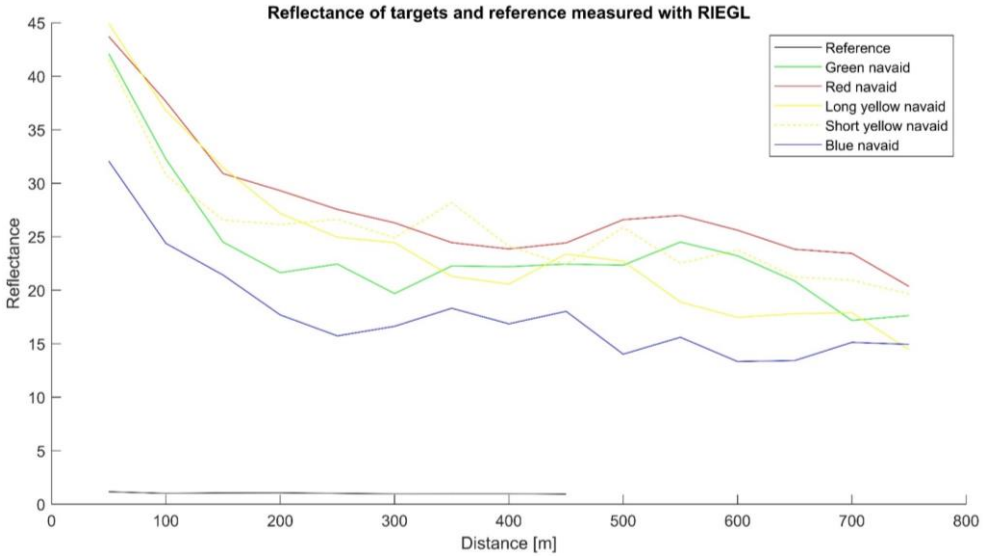

Figure 14: Reflectance reported by the Riegl provide essentially the same information as the amplitude. Blue and green navigation aids perform worse than e.g the red navigation aid across the whole measuring distance.

Results from the Livox are reported as percent of reflectivity compared to a standard target. Figure 15 depicts the reflectivities for each target as a function of distance. Also with Livox, the navigation aids show significantly higher reflectivities compared to the reference target. Due to more modest processing and signal handling capabilities in the Livox, high reflectivity values captured at shorter measuring distances are saturated. Nevertheless, results similar to the Riegl can be observed as blue and green show lower reflectivities. The aluminium reference plate is also showcased in figure 15 and shows the expected exponential decay.

Examining the actual point clouds in appendices B.1 and B.2, one can observe how the increasing distance impacts the accuracy. With Riegl, the point clouds remain remarkably precise, despite the increasing laser spot size due to the beam divergence. However, the targets become ”averaged” as the increasing beam size allows to pick the peak value over a larger area. This results in flattening of the cylindrical structures as the distance is calculated from the peak amplitude value obtained from the reflectors at the center of the navigation aid, even when the beam is directed at the side of the aid. Despite these characteristics, the size of the navigation aids remains remarkably stable and, for example, the size of the green navigation aid can still be estimated to roughly 80cm in diameter at 750m distance. Also the reflection pattern stays remarkably similar across the distance range, despite the averaging effect. One should note, however, that the scanning performed by Riegl at this high resolution is very slow and not necessarily viable choice in all real-time scenarios.

Due to significantly lower angular accuracy in the Livox, the point clouds become increasingly erratic at longer distances; The reflectivity values become spatially randomized due to the noise in angular data. This also causes the size and reflector patterns to become heavily distorted.

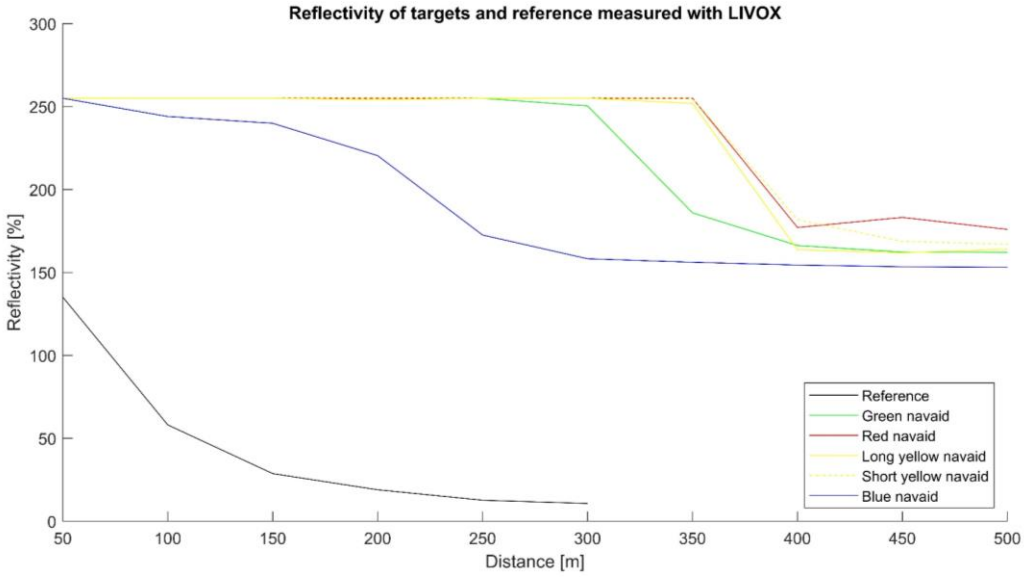

Figure 15: Peak reflectivities of the targets and reference measured with LIVOX as a function of distance. 20 highest reflectivity points were calculated from each target and averaged for each distance. Livox appears to saturate at short distances. Reference target follows the typical exponential decay commonly observed in Lambertian type surfaces. Blue navigation aid exhibits a slightly lower reflectivity. This may be partly due to the materials. A more significant factor is likely the reflector densities and incidence angles. Also green navigation aid appears to have lower reflectivity, but due to the saturation, this is not verifiable for shorter distances.

4 Perspectives on the detection probabilities of navigation aids

Estimating the probability that a given lidar detects a maritime target is a rather involved task. Parallels can be made with radars, for which target detection has been studied rather thoroughly. This typically involves calculating or measuring radar cross section (RCS) for a given target at different angles. RCS is essentially an approximate figure which describes how detectable the target is. Similar approach could be taken with navigational aids, if the targets of interest can be measured or estimated via calculation. However, since this type of approach is not yet established practice with lidars, we will describe a basic statistical approach.

In practice, a lidar scans a predetermined area within which the target is. For a single lidar pulse, given a totally random pulse direction, the probability of detecting the target is roughly the ratio of the target surface to the scan area. For example, the reflecting area of the green navigation aid depicted in previous chapter is roughly 80cm wide and 40cm high, resulting in $0.32m^2$ surface area. Given the conical scanning pattern of the Livox Tele-15 with roughly 15° field of view, the area scanned is given by the equation

$$A = 2\pi r^2 \, (1 - cos(7.5°)) \approx 0.0538 r^2, \qquad (1)$$

where r is the distance from the lidar. Hence the probability is approximately

$$P \approx \frac{0{,}32}{0{,}0538 r^2} \qquad (2)$$

At 100m distance this results in a probability of roughly 0.0005953. A geometric distribution approach can then be used to calculate probability mass function and cumulative distribution function defined by the equations

$$PMF = (1-p)^{k-1} \, p \qquad (3)$$

$$CDF = 1-(1-p)^k \qquad (4)$$

in which p is the probability and k the number of pulses sent by the lidar. These equations allow to evaluate how many pulses are required to get one detection of the target at a certain probability level. Graph of the cumulative distribution function for the given example is depicted in figure 16.

Given the typical pulse rates of modern lidars, detection of the target of the example will typically occur in a fraction of a second. Similar approach can then further be used to calculate how many pulses are required to get a defined number of reflections from the target as single echoes are generally not enough for reliable target identification. The amount of echoes required from a navigation aid for reliable vessel navigation is somewhat philosophical question as it entails assessing required identification accuracy and speed, amongst other things, for various scenarios and use cases. However, since the navigation aids provide very high reflectivity, these can typically be separated from the surroundings simply due to the intensity.

In reality, the given approach assumes stochastic behaviour of the scanning, which may or may not hold true depending on a number of factors. In most cases, the scanning patterns are not random, and the lidar covers the scanning area faster. However, due to, for example, movement of the platform, the random approximation may be relatively good for most cases and especially at long range.

A further problem arises from possible synchronization issues, which can occur in stationary situations. Due to finite angular resolution, a target may be skipped during a scan. If the scan pattern stays spatially synchronized, the target may not be detected at all. The phenomena is well known within the field of radars. These issues can be avoided with e.g. slightly varying scanning patterns or e.g. via platform movement, but it is nevertheless possible that these happen or at least the detection time becomes very long.

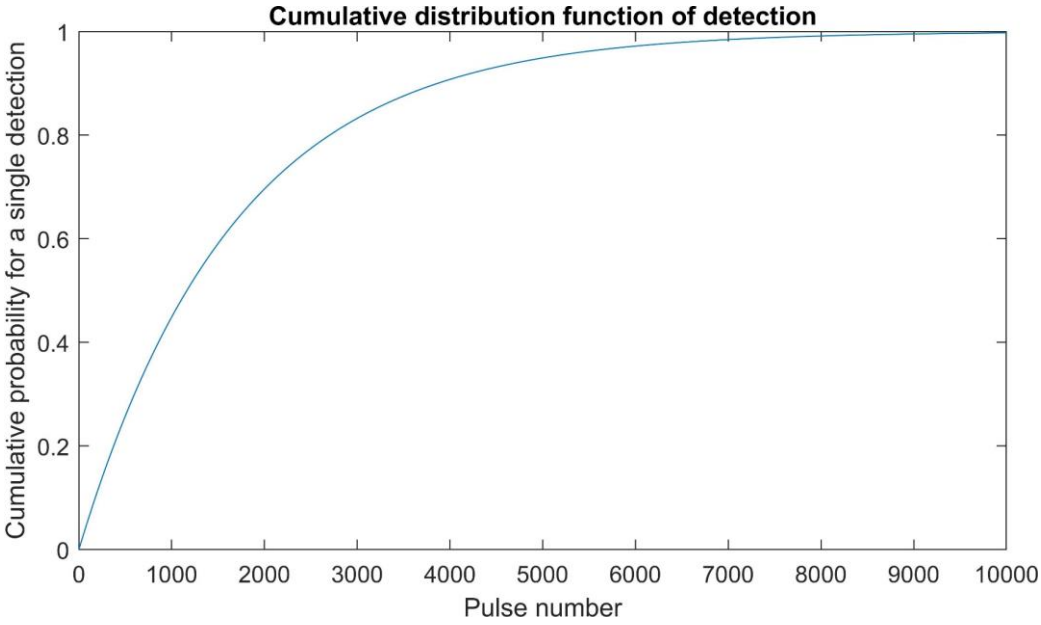

Figure 16: Cumulative distribution function for a single detection of a navigation aid.

Still a further omission of the example is that the target surface area visible for the lidar decreases as the range increases. This can be accommodated in the equations if, for example, we know the minimum required reflectivity and how the target reflectivity behaves as a function of distance and e.g. weather conditions. Point clouds presented in B.1 for the various navigation aids could be utilized for approximations, as we can observe the decay in reflectivity across the measuring distance. Hence, we can construct a function which estimates the surface area of the target as a function of distance and replace the constant target area in the above equations with this function. Furthermore, the beam divergence needs to be included, but this is also relatively straightforward. More profound problem is that for truly accurate estimation we would also need to know the laser beam profile. As the intensity typically is higher at the center of the beam and drops towards the edge, this profile has an impact together with the beam diver- gence and attenuation of the reflector materials at the sides of navigation aid for the resulting detectable area of the navigation aid at a given range. Unfortunately, the beam profiles are often not specified by the manufacturers and hence it is not always possible to take this into account. Thorough measurements would be required for each lidar to assess the impact of beam profile properly. In many cases, gaussian, supergaussian and simiar beam profiles could be utilized for

generalized approximation. Lastly, we would also need to model the receiver aperture size or focusing characteristics, although these are likely similar or larger than the beam divergence. Nonetheless, given that these figures can be measured or calculated, more precise calculations for the detection probability can be established relatively easily.

Realistic probability calculation would also need to further include estimates of e.g. the impact of rough seas, where part of the reflecting surface of the aid may be covered periodically by waves.

5 Views on lidar eye-safety

5.1 Laser eye-safety

Light radiation can cause adverse effects on humans, mostly in the form of temporary or permanent impairment of vision and various effects on skin, such as skin burns. Compared to other light sources, lasers are generally more potent and can cause damage at significantly lower power levels due to the coherent, monochromatic and collimated nature. Hence, safety is of paramount importance when lasers are operated in the vicinity of humans and animals. [6][7][8][9]

European union has established directives to regulate safety of artificial optical radiation. For lasers, the safety related aspects are covered in EN 60825 series documents. The EU directive is based on the International Electrotechnical Commission (IEC) 60825 document, which was adopted essentially 'as is' by the EU. The IEC 60825 serves as the basis for other national standards as well and sets the basic commercial lidar operating limits. Use of lasers in specific fields, e.g. in medicine, may be further regulated by more specific guidelines and directives. [6][10]

Eye-safety of lasers is a complicated issue, as damage and other adverse effects vary depending on the wavelength, pulsewidth, pulse frequency and pulse energy as well as beam divergence, viewing distance and other viewing conditions. In general, damage occurs at tissues when the energy or power per area is high enough for thermal or photochemical reactions to happen. [9][11][12]

Different parts of the human eye attenuate and react differently to ultraviolet, visual and infra-red wavelengths. In essence, human eye adapts and reacts only to light intensity at visible wavelengths. For example, the blink reflex does not occur at infra-red wavelengths, leaving the eye susceptible to prolonged exposure to radiation of said wavelengths. [9][11][12]

Ultraviolet (UV) light does not penetrate deep into the eye as cornea is highly absorping at UV-wavelengths. Hence, high UV light levels mostly cause damage at the cornea, in the form of photokeratitis, photochemical cataract, lesions and opaque scarring.

Visual and near infra-red wavelengths, between 400 and 1400nm are transmitted and focused by the crystalline lens on to the retina. Excessive radiation at these wavelengths can cause permanent damage to the retina. Perfectly collimated light entering an eye with normal vision, will focus on to a very small area, resulting in very high power and energy densities. Consequently, even a very low light level can cause damage. While the damaged area remains small, certain areas, such as the fovea, are essentially very small and hence, significant vision impairment can happen even with spatially miniscule damaged region. [9][11][12]

Human eye has relatively good correction of aberrations due to non-uniform refraction in the cornea and lens. However, chromatic aberration can not be fully removed and hence, different wavelengths will have slightly different focal length, resulting different spot sizes at the retina. Considering individual (physiological) and circumstantial differences, wavelength dependent damage tresholds are, therefore, approximations. In addition, as the amount of radiation entering the

vitreous body of the eye depends on the dilation of the pupil, occurrence of damage may depend on the general or ambient lighting conditions for which the eye, i.e. the pupil, has adapted. Similar to the blink reflex, IR wavelengths may not provide pupil response and hence, the eye can absorp high IR flux in dark ambient conditions.

Absorption of the cornea increases again at wavelengths above 1400nm with distintive peaks at around 1400-1500nm and 2000nm. Hence, damage from radiation above 1400nm occurs mostly at the cornea in the form of cataract and corneal burn.

Due to the highly wavelength dependent damage tresholds of the human eye, lasers operating above 1400nm can generally have significantly higher output power compared to lasers below 1400nm. The exact levels depend on other factors, especially on pulse duration and pulse energy. In general, low instantaneous pulse energy will allow higher average output power. Increasing the pulse duration will hence allow higher power and consequently longer range with a degradation in the distance accuracy. [8][9]

The IEC 60825 standard and the equivalent EU standard define the applicable maximum permissible exposure (MPE) in both W/cm^2 and J/cm^2 as a function of wavelength for the safe operation of lasers. Due to the number of factors and uncertainty involved, these safety limits are generally very conservative. [10]

To simplify the use of laser based equipment, these are classified to different safety levels depending on the average output or per pulse power level and operating wavelength. This classification scheme allows easy assessment of the required safety precautions to operate the given laser unit. The newest 60825 based standard defines 4 main classes with few subclasses for lasers, namely, classes: 1, 1M, 2, 2M, 3R, 3B & 4. [10]

- Class 1 lasers are considered safe to operate essentially at any conditions (intended for the device) and should not cause any health effects, either due to the very low level radiation (below MPE), or due to the radiation being enclosed in the unit.

- Class 1M devices may have higher power levels compared to class 1, but due to e.g. optics and beam diameter or divergence, the radiation does not exceed the MPE. However, if the beam is viewed through focusing optics, the MPE may be exceeded and hence, the safe use of these lasers in contingent on the condition that the beam is not viewed through optics with focusing capabilities.

- Class 2 devices operate below 1mW at visible wavelengths between 400 and 700nm, and are eye-safe, mostly due to the response of the eye, e.g. the blink reflex.

- Class 2M devices are equivalent to class 2 with limitations imposed on the beam viewing through optical instruments similar to class 1M.

- Class 3R devices are medium power devices that may exceed the MPE levels and can present low to medium risks of injury when directly viewing the beam.

- Class 3B devices are considered dangerous for direct beam viewing. Diffuse reflections are generally considered harmless.

- Class 4 devices are the highest power devices and can cause permanent damage to vision and skin even with indirect or diffuse exposure.

Vast majority of commercial lidars fall under the class 1 devices. Since most lidars operate at infra-red wavelengths, class 2 is rarely applicable. Handful of lidars, typically aimed at long range survey tasks are beyond class 2, such as the 3B classified very long range Riegl VZ-6000 lidar.

Due to beam divergence, the energy or power density decreases quite rapidly as a function of distance from the lidar unit, and hence, a lidar classified as safe at short distance is even less likely to cause damage at longer range. Considering safety in maritime use, the targets of concern are generally humans and birds. In most cases, lidar placement can be designed in such a way that close range human exposure is minimized by e.g. placing the lidars above eye-line on the deck. For birds, on the other hand, this type of approach is unlikely to work.

Of a particularly significant concern is the increasing number of lidars and the possibility of exposure to several lidar beams simultaneously. As noted, lidars operating between 700-1400nm can cause retinal burn while lidars above 1400nm are mostly concerned with corneal burn damage. For infrared lidars operating below 1400nm, the focusing properties of eye make it practically impossible for two beams originating from different locations to focus on the same spot on the retina. Hence, retinal damage due to cumulative superposition of several beams is very unlikely with these wavelengths, unless there are lidars that are placed very close to each other. On the other hand, several beams originating from various lidars operating at around 1500nm could very well coincide at the cornea, causing damage due to cumulative power levels. The probability for calculating such occurrence is relatively complex as this would need to assess number of operating parameters. Nevertheless, it is a likely occurrence given enough time in a place where multiple lidars have overlapping scan areas. Unfortunately, no large scale studies have yet been made to assess these risks.

6 Conclusions

The measured reflector materials perform very well across the 800-1800nm range and furthermore, provide high retroreflective characteristics, which makes them very good targets for commercial lidars operating at the said wavelength range. During the measurements, it became evident that longer distance detection of navigation aids equipped with these reflector materials is less challenging than expected. The high retroreflectiveness makes these targets visible beyond the range of most commercial lidars when operating in good conditions. It is likely that these materials can be detected up to several kilometers on the basis of reflectivity alone. The bigger obstacle to detecting these targets comes from the limited angular resolution, pulse rate and scanning rate of existing lidars. Especially the angular resolution and pulse rate are limiting factors at longer range. Hence, fast (i.e. real-time application) and reliable detection of these targets at long distance will likely be achieved by using a number of lidars each scanning a small sector of the total field of view. Survey type tasks, for example, examining the condition and location of a navigation aid remotely (in good weather conditions), will be limited mostly by the angular resolution and accuracy of the device as well as the beam divergence. If a survey is performed from a moving platform, also the compensation of the platform movement needs to be very accurate in order to achieve results similar to the millidegree accuracy shown by the tests done with the Riegl lidar. However, optimising the reflector material and navigation aid patterns could still be very beneficial as the detection range will be limited in adverse weather conditions. In adverse conditions, such as heavy fog, the detection distance will likely be limited mostly by the receivers capability to capture weak echoes, for which proper navigation aid design could provide alleviation.

Due to the rapid development of lidar technology within the last decade and the trends observable in the industry, the lidar prices, performance and prevalence will improve rapidly for the foreseeable future. Current selection of commercial lidars is poorly optimized for maritime use as this environment is somewhat different from the traditional fields utilizing lidar. Especially the range, angular accuracy and pulse rates would need to be optimized for maritime use. Also weather proofing of the lidar would need to be implemented specifically for maritime conditions. With the emergence of autonomous shipping, it is highly likely that we will see these maritime optimized lidars in the future.

6.1 Recommendations for improvements

Based on the observations detailed in this report, a significant factor in the amount of light emitted back to the lidar is the incidence angle of the reflector material. In the tested navigation aids, the spatial density of the reflector strips varied, and this was likely a significant contributor to the differences in the reflectivity of the targets. Providing denser strip pattern makes it more probable that the lidar beam will hit a reflector with very small incidence angle, hence, improving the detection possibilities. Denser strip configuration will also increase the overall amount of reflective surface area for a given sized aid, which will increase the light flux at the receiver. However, the impact of reflector surface size is not necessarily linear as it depends on the sensing element in the lidar as well as the processing method of the signal. In traditional avalanche photodiode-based systems, the relationship between light flux and detection probability is somewhat linear, whereas single

photon detecting, e.g. geiger mode photodiode based receivers behave in more discretized way. Nevertheless, the amount of reflective surface will also be an important factor and would benefit from increased size. However, it would seem more important to increase the overall size of the navigation aid, which would spread the reflectors on wider area, making them more detectable for lidars with finite angular resolution.

Considering the tested reflector materials, the most obvious conclusion is that there are observable differences between the manufacturers in the reflectivity of the material, as well as in the retroreflective properties. Furthermore, materials manufactured by 3M appear to have retroreflective capabilities which vary spatially depending on the reflector pattern alignment. This raises and important question, namely, should the navigation reflectors be optimized in such a way that the retroreflective performance is max imized in the horizontal direction? Considering the way the 3M strips are embedded in the navigation aids and the way reflectivity of these reflectors decrease at the sides of the navigation aids, it would seem logical that higher retroreflective capability at high incidence angles would increase the detection capability the most. It might be beneficial to utilize material that has higher retroreflective capabilities, even if the absolute reflectivity of that material is slightly lower. However, this is debatable and depend on the application requirements: lower overall reflectivity will decrease the range at which the target can be detected, while increased surface area will increase the probability of detection within a given time period. Further studies close to the detection limits of lidars would be required together with application assessment to provide definite answer. In the current way of embedding the 3M strips in the navigation aids, a substantial portion of the reflector material is furthermore shadowed by the walls of the recess, decreasing further the reflective area. Considering these aspects, it is highly likely, that reflector strips wrapped around the navigation aid in the horizontal plane would provide better performance.

Lidar measurements at surface level often suffer from optical distortion and refraction in the air caused by temperature differentials between surface and air. Furthermore, measurements near water surface are often further degraded by the moisture content in the vicinity of the surface due to evaporation. These effects are pronounced near the surface up to several meters, and especially in calm (still, non windy) conditions. Due to this, lidars should be placed as high as possible in vessels utilizing them. Consequently, providing retroreflectivity also in the upwards direction from the horizontal plane could be considered beneficial.

Also, the movement of the navigation aids should be taken into account in these evaluations. For example, tilting of the navigation aid due to strong winds may change the detectability to a certain degree. Hence, slightly different reflector characteristics might be suitable between stable aids and aids prone to tilting. For stable platforms, the retroreflective directions should be aimed at and above horizontal plane. For tilting aids the retroreflective pattern should be more omnipolar.

For further studies, evaluating different sized reflectors and strip densities with various alignments and arrangements could be considered beneficial. Especially beneficial would be to study the visibility of horizontally continuous reflector segments. Further studies could also include tests on the ability of fullwaveform lidars to analyze the echo waveform shape and detect the reflector materials based on this waveform. The Riegl VZ-400i utilized in the measurements has this capability, but this analysis was not implemented during the work due to time constraints.

References

/1/ S. Thombre, Z. Zhao, H. Ramm-Schmidt, J. M. V. García, T. Malkamäki, S. Nikolskiy, T. Hammar- berg, H. Nuortie, M. Z. H. Bhuiyan, S. Särkkä, and V. V. Lehtola. Sensors and ai techniques for situational awareness in autonomous ships: A review. IEEE Transactions on Intelligent Transportation Systems, pages 1–20, 2020.

/2/ Isaac I. Kim, Bruce McArthur, and Eric J. Korevaar. Comparison of laser beam propagation at 785 nm and 1550 nm in fog and haze for optical wireless communications. In Eric J. Korevaar, editor, Optical Wireless Communications III, volume 4214, pages 26 – 37. International Society for Optics and Photonics, SPIE, 2001.

/3/ Tuomo Malkamäki, Sanna Kaasalainen, and Julian Ilinca. Portable hyperspectral lidar utilizing 5 ghz multichannel full waveform digitization. Opt. Express, 27(8): A468–A480, Apr 2019.

/4/ Teemu Hakala, Juha Suomalainen, Sanna Kaasalainen, and Yuwei Chen. Full waveform hyperspectral lidar for terrestrial laser scanning. Opt. Express, 20(7):7119–7127, Mar 2012.

/5/ Martin Pfennigbauer and Andreas Ullrich. Improving quality of laser scanning data acquisition through calibrated amplitude and pulse deviation measurement. In Monte D. Turner and Gary W. Kamerman, editors, Laser Radar Technology and Applications XV, volume 7684, pages 463 – 472.

/6/ Kotzur, Sebastian, Siegfried Wahl, and Annette Frederiksen. "Retinal image analysis for eye safety evaluations of products emitting optical radiation." *Optical Interactions with Tissue and Cells XXXI*. Vol. 11238. International Society for Optics and Photonics, 2020.

/7/ Williamson, Craig A., et al. "Wavelength and ambient luminance dependence of laser eye dazzle." *Applied optics* 56.29 (2017): 8135-8147.

/8/ McCally, Russell L., et al. "Laser eye safety research at APL." *Johns Hopkins APL technical digest* 26.1 (2005): 46-55. Laser safety, October 2020.

/9/ Barkana, Yaniv, and Michael Belkin. "Laser eye injuries." *Survey of ophthalmology* 44.6 (2000): 459-478. Bird vision, January 2021.

/10/ De Luca, Daniele, Ines Delfino, and Maria Lepore. "Laser safety standards and measurements of hazard parameters for medical lasers." *International Journal of Optics and Applications* 2.6 (2012): 80-86.

/11/ Yu, Zhaohua. *Damage mechanisms for near-infrared radiation induced cataract*. Diss. Acta Universitatis Upsaliensis, 2017.

/12/ Kourkoumelis, Nikolaos, and Margaret Tzaphlidou. "Eye safety related to near infrared radiation exposure to biometric devices." *TheScientificWorld JOURNAL* 11 (2011): 520-52

Finnish Transport
Infrastructure Agency

ISSN 2490-0745
ISBN 978-952-317-869-4
www.vayla.fi